Cardiovascular Diabetology

RESEARCH

Open Access

Piezo1 deletion mitigates diabetic cardiomyopathy by maintaining mitochondrial dynamics via ERK/Drp1 pathway

Weipin Niu[1,2], Xin Liu[1,3], Bo Deng[4], Tianying Hong[1], Cuifen Wang[1], Yameng Yan[1], Jiali Liu[1], Yuehua Jiang[2*] and Jing Li[1,5,6,7*]

Abstract

Objective Increasing evidence highlights the critical role of Piezo1 in cardiovascular diseases, with its expression upregulated in diabetic heart. However, the involvement of Piezo1 in the pathogenesis of diabetic cardiomyopathy (DCM) remains unclear. This study aims to elucidate the regulatory role of Piezo1 in mitochondrial dynamics within the context of DCM and to investigate the underlying mechanisms.

Methods We constructed cardiac-specific knockout of Piezo1 (*Piezo1*$^{\Delta Myh6}$) mice. Type 1 diabetes was induced using streptozotocin (STZ) injection while type 2 diabetes was established through a high-fat diet combined with STZ. Echocardiography assessed left ventricular function, histological evaluations used HE and Masson staining to examine cardiac pathology in *Piezo1*$^{fl/fl}$ controls, *Piezo1*$^{\Delta Myh6}$ controls, *Piezo1*$^{fl/fl}$ diabetic and *Piezo1*$^{\Delta Myh6}$ diabetic mice. Mitochondrial function including oxygen species level, mitochondrial morphology, and respiration rate were also assessed.

Results Our findings revealed that Piezo1 expression was upregulated in the myocardium of diabetic mice and in high-glucose-treated cells. Cardiac-specific knockout of Piezo1 improved cardiac dysfunction and ameliorated cardiac fibrosis in diabetic mice. Moreover, Piezo1 deficiency also attenuated mitochondrial impairment. *Piezo1*$^{fl/fl}$ diabetic mice exhibited increased calpain activity and excessive mitochondrial fission mediated by Drp1 and obvious reduced fusion; however, Piezo1 deficiency restored calpain levels and mitochondrial dysfunction. These observations were also corroborated in H9C2 cells and neonatal mouse cardiomyocytes. Cardiac-specific knockout of Piezo1 increased phosphorylation of Drp1 and ERK1/2 in vivo and in vitro. Piezo1 knockout or treatment with inhibitor improved mitochondrial function.

*Correspondence:
Yuehua Jiang
jiang_yuehua@hotmail.com
Jing Li
bmsjingl@gzucm.edu.cn

Full list of author information is available at the end of the article

Conclusions This study provides the first evidence that Piezo1 is elevated in DCM through the modulation of mitochondrial dynamics, which is reversed by Piezo1 deficiency. Thus, Piezo1 inhibition may provide a promising therapeutic strategy for the treatment of DCM.

Graphic abstract In cardiomyocytes of Piezo1$^{fl/fl}$ DCM mice, increased Ca^{2+} entry upregulates calpain activity, and phosphorylated level of ERK1/2 and Drp1. Therefore, increased mitochondrial fission is shown in DCM hearts. Whereas, cardiomyocyte-specific knockout of Piezo1 alleviates mitochondrial dysfunction.

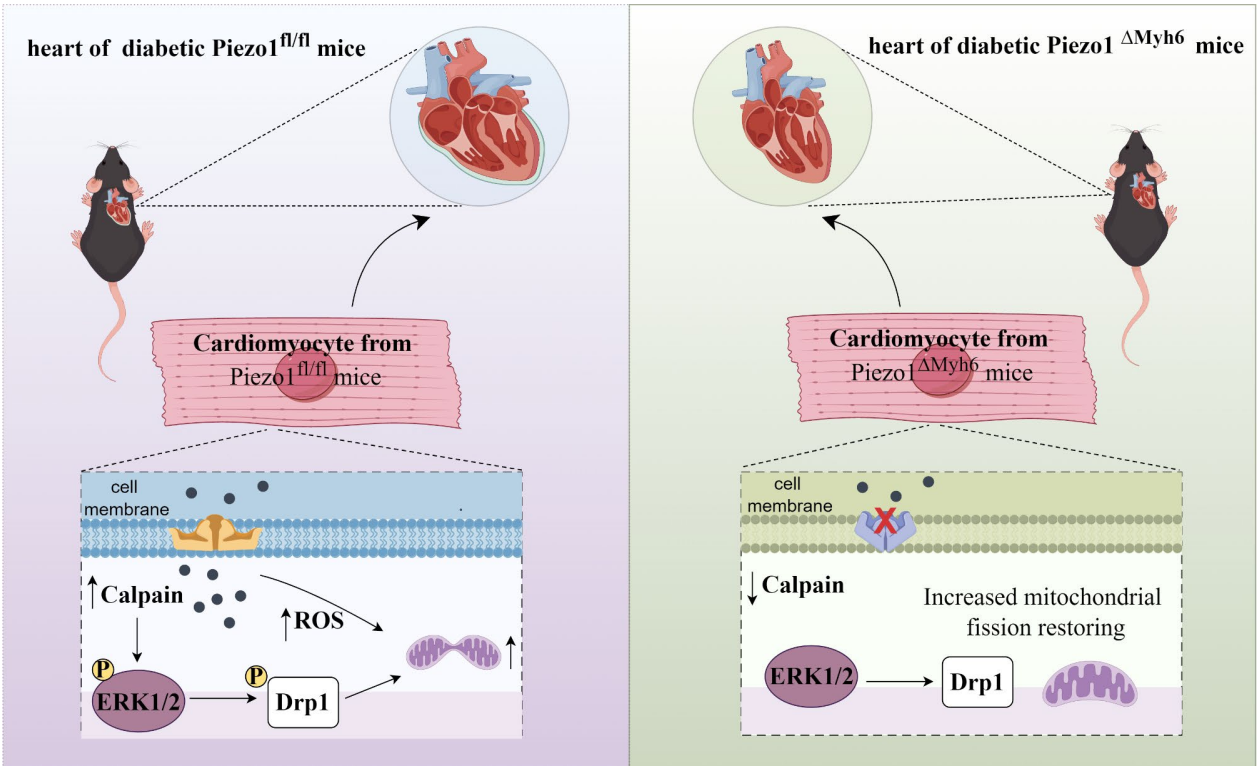

Keywords Diabetic cardiomyopathy, Mitochondrial dynamics, Piezo1, ERK1/2, Drp1

Introduction

The incidence of both type 1 and type 2 diabetes mellitus (T1DM and T2DM) continues to rise globally. DM complications, including neuropathy, cardiovascular changes and nephropathy, are major causes of mortality and morbidity among diabetic patients, placing a substantial burden on global public health. Of particular concern is diabetic cardiomyopathy (DCM), characterized by a series of abnormalities in myocardial structure and function due to insulin resistance, inflammation, altered lipid metabolism, and mitochondrial impairment. These manifest as myocardial hypertrophy, interstitial fibrosis, and diastolic dysfunction [1]. Thus, there is an urgent need to identify novel therapeutic targets and deepen our understanding of the pathological and molecular mechanisms underlying DCM.

Piezo1, identified as a mechanosensitive ion channel within the past decade [2], plays a vital role in a multitude of physiological processes, such as innate immunity [3], blood pressure regulation [4, 5], stem cell aging [6], cell fate determination [7, 8] and cardiovascular homeostasis [9–11]. The Piezo1 protein is abundantly expressed in myocardial tissue, where it converts mechanical stress into Ca^{2+} signaling [12, 13]. Hydrophobic Yoda1 can directly bind to Piezo1, resulting in Piezo1 activation; but non-specific blockers including spider toxin GsMTx4 and ruthenium red can block Piezo1 activation [14]. Previous study has demonstrated a significant increase in Piezo1 levels in adult mice subject to pressure overload-induced cardiac hypertrophy [15]. Moreover, cardiac-specific deletion of Piezo1 inhibited the activation of the Ca^{2+}/calmodulin-dependent protein kinase II (CaMKII), thereby preventing a decline in cardiac function. Notably, Piezo1 expression is elevated in islets from humans and mice with T2DM, as well, impaired glucose tolerance and reduced insulin secretion present in β-cell-specific *Piezo1*-knockout mice [16]. Hence, investigating the role

of Piezo1 in cardiac dysfunction associated with DCM is imperative in future study.

Mitochondrial dysfunction exerts a crucial role in the pathogenesis of DCM [17]. Mitochondria, the double-membrane organelles, produce adenosine triphosphate (ATP) using glucose and oxygen in cardiomyocyte. Emerging evidence suggests that hyperglycemia and insulin resistance disrupt mitochondrial dynamics by promoting mitochondrial fission and inhibiting mitochondrial fusion [18]. Mitochondrial fusion is modulated by mitofusin-1 (Mfn1), mitofusin-2 (Mfn2), and optic atrophy 1 (Opa-1), while fission is primarily controlled by mitochondrial fission protein 1 (Fis1), dynamin-related protein 1 (Drp1) and mitochondrial fission factor (Mff) [19]. Excessive mitochondrial fission in diabetic hearts increases mitochondrial numbers while reducing their size, leading to excessive reactive oxygen species (ROS) production and contributing to mitochondrial dysfunction [20].

In this study, we demonstrated the cardioprotective effect of Piezo1 in DCM by improving diastolic and systolic function, and ameliorating cardiac fibrosis. Our findings indicate that increased Piezo1 expression leads to calcium influx in cardiomyocytes, subsequently elevating calpain activity and activating extracellular signal-regulated kinase (ERK1/2) signaling. These result in Drp1 phosphorylation, which promotes mitochondrial fission and mitochondrial dysfunction. Cardiac-specific deletion of Piezo1 ameliorates cardiac remodeling and mitochondrial dysfunction, uncovering a Piezo1-regulated mitochondrial homeostasis mechanism linked to ERK/Drp1 axis in diabetic hearts, thus highlighting Piezo1 as a therapeutic potential target in DCM treatment.

Materials and methods

Animal studies and ethics

Conditional cardiac-specific Piezo1 knockout mice (*Piezo1*$^{\Delta Myh6}$) were created by crossing *Piezo1*$^{fl/fl}$ mice (Piezo1tm2.1Apat/J) from Jackson Laboratory with Myh6-Cre transgenic mice (A1cf$^{Tg(Myh6-cre/Esr1*)1Jmk}$/J). Additionally, mice expressing a C-terminal fusion of *Piezo1* with a tandem-dimer *Tomato* sequence (*dtT*; *Piezo1*$^{dtT/dtT}$ mice) [21] were also sourced from Jackson Laboratory. All animal experiments were adhered to the guidelines of the Care and Use of Laboratory Animals and were permitted by the Animal Care and Use Committee of Shandong University of Traditional Chinese Medicine (approval number: SDUTCM20230215211). Mice was genotyped using PCR with genomic DNA isolated from mouse tails with the following primers: *Myh6-cre* 5'-ATGACAGACAGATCCCTCCTATCTCC-3' (forward); *Myh6-cre* 5'-CTCATCACTCGTTGCATCAT CGAC-3' (reverse); mouse *Tomato* (mutant) 5'- CACCT GTTCCTGTACGGCATGGAC – 3', *Tomato* (common) 5'- GTCCCTTTGACAGCAGCATC – 3', (wildtype) 5' - A CGCCAAGCTCATCTTCCT – 3'.

Experimental animal models

All mice were maintained under specific-pathogen-free conditions (12 h day-night cycle) at appropriate temperature and humidity, with unrestricted access to sterilized water and food.

T1DM mice

The experimental design flowchart was illustrated in Fig. 2A. To examine the expression level of Piezo1 in DCM, twenty 8-week old male *Piezo1*$^{dtT/dtT}$ mice were utilized to construct diabetic models via intraperitoneal injections of streptozotocin (STZ, dissolved in citrate buffer, 0.1 mM, pH = 4.5, MCE, USA) at a dosage of 55 mg/kg daily for 5 consecutive days. Mice in the control group received intraperitoneal injection of citrate buffer. After 2 weeks, T1DM mice were confirmed in mice exhibiting fasting blood glucose (FBG) ≥ 16.7 mM/L for two consecutive days. All mice were subsequently maintained for an additional 14 weeks prior to sample collection. To further investigate the role of Piezo1 in DCM, C57BL/6J mice (Vital River Laboratory Animal Technology Co., Ltd, China) were also used to establish T1DM (Fig. 8A). Twelve weeks after DCM induction, the Piezo1 agonist Yoda1 (MCE, USA) was administrated to diabetic mice via intraperitoneal injection (80 μg/kg, once daily for 4 weeks) [22].

HFD/STZ induced diabetic mice

To estimate the levels of Piezo1 in T2DM and assess the impact of Piezo1 knockout on cardiac function in diabetic context, *Piezo1*$^{dtT/dtT}$, *Piezo1*$^{\Delta Myh6}$ and *Piezo1*$^{fl/fl}$ mice aged 3 weeks were subjected to construct T2DM model through high-fat diet (HFD, 60 kcal% fat; Research Diets, Inc, USA; Supplementary file 3: Table S1) for 6 weeks followed by intraperitoneal STZ injections at a dose of 35 mg/kg for three consecutive days. All mice were randomly divided into six groups ($n = 10$ per group): *Piezo1*$^{dtT/dtT}$ mice fed chow diet group (*Piezo1*$^{dtT/dtT}$ control group), *Piezo1*$^{dtT/dtT}$ mice fed HFD group (*Piezo1*$^{dtT/dtT}$ T2DM group), *Piezo1*$^{fl/fl}$ fed chow diet group (*Piezo1*$^{fl/fl}$ + control), *Piezo1*$^{fl/fl}$ fed HFD group (*Piezo1*$^{fl/fl}$ + HFD), *Piezo1*$^{\Delta Myh6}$ fed chow diet group (*Piezo1*$^{\Delta Myh6}$ + control), *Piezo1*$^{\Delta Myh6}$ fed HFD group (*Piezo1*$^{\Delta Myh6}$ + HFD). Mice with random blood glucose ≥ 16.7 mM were selected for subsequent studies and continued fed with HFD diet for additional 16 weeks.

Intraperitoneal glucose tolerance test (IPGTT)

At the end of treatment, IPGTT was performed in all mice after overnight fasting. All T2DM mice were received a 2 mg/g intraperitoneal glucose injection, with

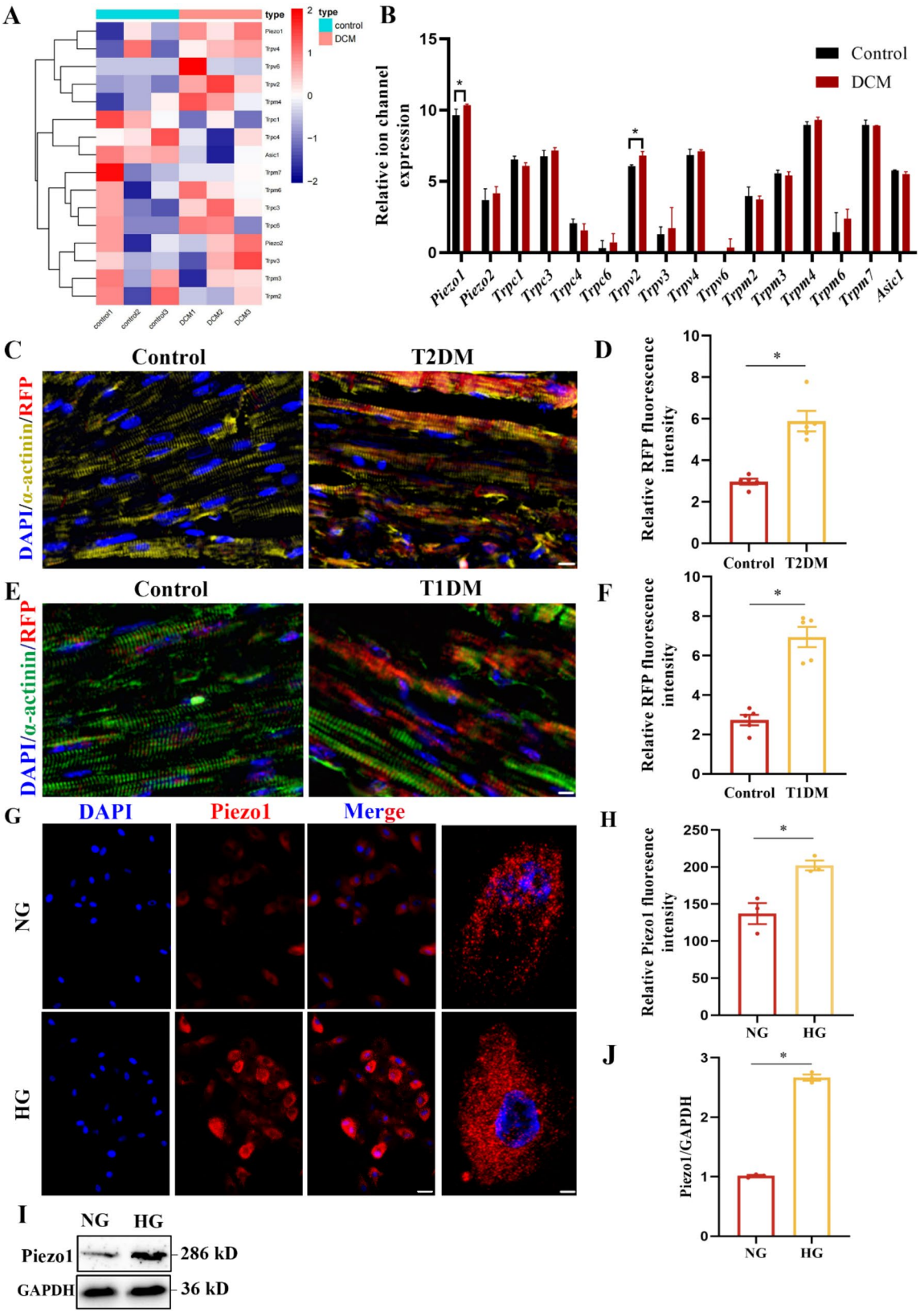

Fig. 1 (See legend on next page.)

(See figure on previous page.)

Fig. 1 Increased Piezo1 expression in the heart of diabetic mice and high glucose-treated H9C2 cells. (**A**) Heatmap showing differentially expressed ion channel genes in normal and HFD/STZ-induced DCM hearts ($n=3$). (**B**) Relative mRNA levels of ion channel genes in hearts from normal and HFD/STZ induced DCM mice. (**C**) Representative images of immunofluorescence staining of RFP in the heart of T2DM mice ($n=5$). Scale bar, 20 μm. (**D**) Quantification of fluorescence intensity of RFP in (**C**). (**E**) Representative images of immunofluorescence staining of RFP in the heart of T1DM mice ($n=5$). Scale bar, 20 μm. (**F**) Quantification of fluorescence intensity of RFP in (**E**). (**G**) Representative images of immunofluorescence staining of Piezo1 (red) in normal glucose (NG) or high glucose (HG) treated H9C2 cells ($n=3$). The nuclei were co-stained with DAPI (blue). Scale bar, 50 μm. Several cells were also represented using oil immersion lens (Scale bar, 10 μm). (**H**) Quantification of fluorescence intensity of Piezo1 in (**G**). (**I**) Western blot for Piezo1 in H9C2 cells treated by high glucose (HG) compared with normal glucose (NG) ($n=3$). (**J**) Quantification of western blot. *$P<0.05$

blood glucose levels monitored pre-injection (0 min) as well as at 30, 60, 90 and 120 min post-injection.

Echocardiography

Following anesthesia with 2% inhaled isoflurane, transthoracic echocardiography was conducted at the end of the experiment using a VINNO ultrasound diagnostic instrument (VINNO, Suzhou, China). Parasternal long-axis M-mode images were collected and parameters recorded to assess systolic and diastolic cardiac function, including left ventricular (LV) ejection fraction (EF%), LV shortening fraction (FS%), LV internal dimension at diastole (LVID; d), LV internal dimension at systole (LVID; s), LV anterior wall thickness at diastole (LVAW; d), LV anterior wall thickness at systole (LVAW; s), LV posterior wall thickness at diastole (LVPW; d) and LV posterior wall thickness at systole (LVPW; s).

Histological analysis

Heart weight (HW) and tibial length (TL) of all mice were measured to calculate the HW/TL ratio. Following fixation in 4% paraformaldehyde, heart tissues of mice were embedded in paraffin and sectioned to a thickness of 4 μm. Deparaffinized and rehydrated sections were stained with hematoxylin and eosin (H&E, Beyotime Biotech, China), Masson's trichrome (Solarbio, China) and Alexa Fluor 488 labeled wheat germ agglutinin (WGA, Thermo Fisher, USA) staining to assess collagen content and myocardial atrophy according to the manufacturer's instruction.

Immunofluorescence (IF) staining of tissue was conducted to detect Piezo1 expression and collagen levels in cardiomyocytes. Sections were deparaffinized and rehydrated before being blocked with 5% goat serum (Solarbio, China) for 30 min, then incubated with primary antibodies RFP, collagen I and collagen III at 4°C overnight. Subsequent treatments included incubation with secondary antibodies in the following morning, and sections stained with RFP were then incubated with α-actinin antibody to label myocardical tissue. Cells seeded on glass coverslips were fixed in 4% paraformaldehyde for 15 min, blocked with 5% goat serum for 30 min and then incubated with primary antibodies against Piezo1, Tomm20, p-Drp1 (ser616) and OPA1 at 4 °C overnight. Images were acquired with a fluorescent microscope (BZ-X710, KEYENCE, Japan).

Cell culture and treatment

The embryonic rat heart-derived cardiomyocyte-like H9C2 cell line was obtained from the Wuhan Servicebio Technology Co., Ltd. and primary neonatal mouse cardiomyocytes (NMCMs) were isolated from neonatal mice aged 1–3 days. Mouse hearts were obtained and ventricular sections were diced into small pieces, followed by digestion for 8 h at 4 °C with 0.125% trypsin and then for 30 min at 37 °C with 0.5% collagenase II. Cell suspension was obtained via filtering tissue fragments with 40-μm cell strainers (Falcon, USA). Purified cardiomyocytes were collected and culture medium was replaced 24 h later [23]. All cells were cultured in Dulbecco's modified Eagle medium (DMEM) medium (Gibco, Germany) which contained 1 g/L of D-glucose and supplemented with 100 U/ml of penicillin and streptomycin, and 10% fetal bovine serum. In the first part of the in vitro study, to estimate the effect of Piezo1 inhibition on mitochondrial function, after plated in six-well plates or glass coverslips and then starved for 12 h, H9C2 cells were treated with 35 mM D-glucose (Sigma, USA) with 500 μM palmitate (Sigma, USA) in the presence or absence of GsMTx4 (10 μM, MCE, USA) for additional 48 h as HG + PA or GsMTx4 groups, identical concentrations of mannitol as normal glucose (NG) group. In the subsequent phase of the in vitro study, to investigate the effect of Piezo1 deficiency on mitochondrial function, the primary NMCMs were treated with 35 mM D-glucose and 500 μM palmitate or NG for 48 h.

Quantitative real-time polymerase chain reaction (RT-PCR)

Total RNA was extracted from cardiomyocytes or heart tissues using TRIzol Reagent (Invitrogen, USA) following the manufacturer's instructions. Total RNA was reversed into cDNA using ReverTra Ace qPCR RT Kit (Takara, Japan) and quantitative RT-PCR was conducted using SYBR Green Realtime PCR Master Mix (Takara, Japan) on a LightCycler 480 instrument (Roche, Switzerland). β-actin was used as control, and relative gene expression was calculated through the $2^{-\Delta\Delta Ct}$ method. All samples were examined in triplicates. Primer sequences for RT-PCR were listed in Supplementary file 3: Table S2.

Transmission electron microscopy (TEM)

Mitochondrial ultrastructure in myocardial samples was examined by fixing mouse heart tissues with

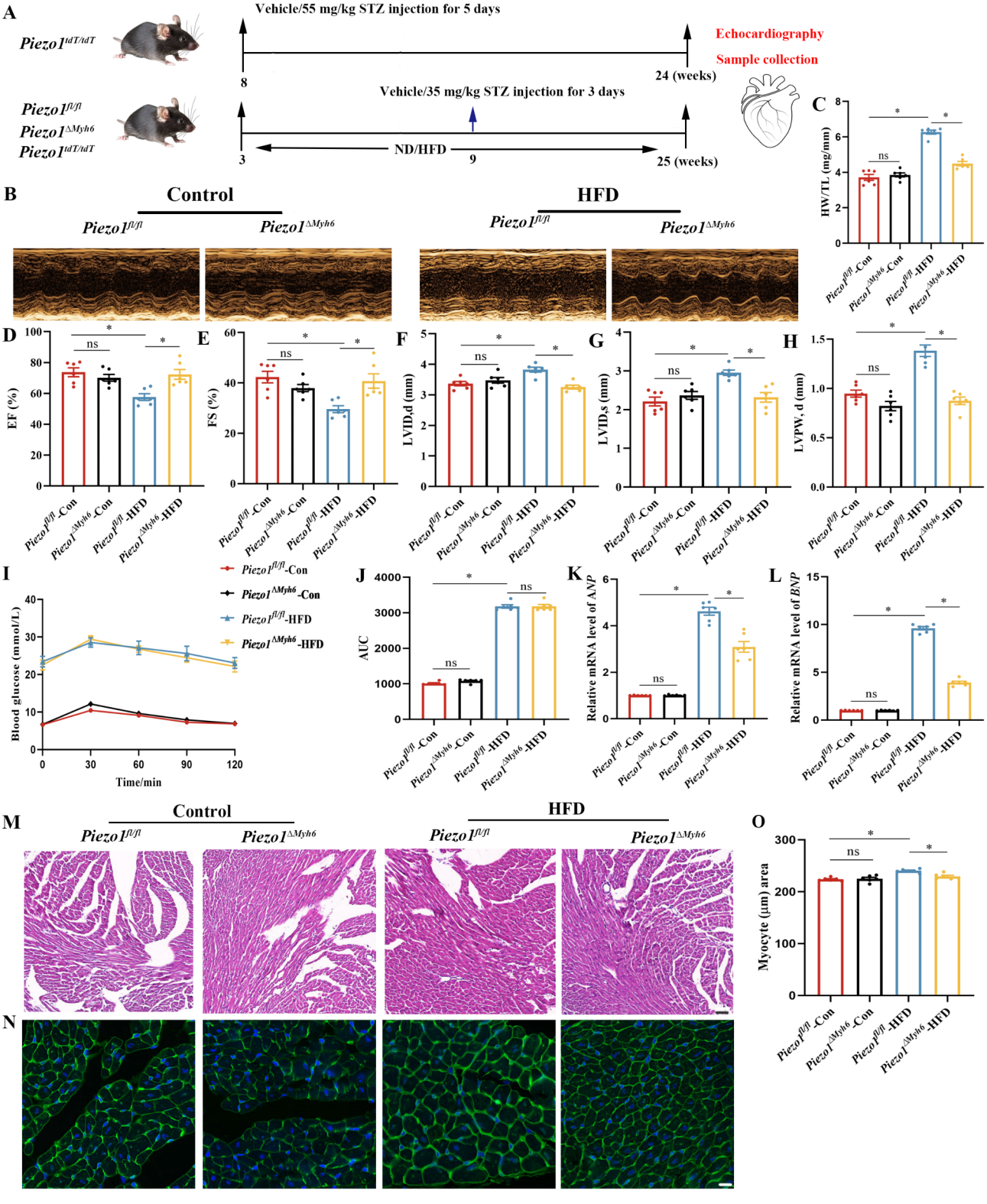

Fig. 2 (See legend on next page.)

(See figure on previous page.)

Fig. 2 Piezo1 deficiency improved left ventricular function and remodeling in diabetic mice. (**A**) Experiment timeline in mice used in this study. (**B**) Representative M-mode echocardiographic images for the mice showing left ventricular diamensions. (**C**) Quantification of the ratio of heart weight (HW) to tibial length (TL) in four groups of mice ($n=6$). (**D**, **E**) Quantification of left ventricular ejection fraction (EF) and fractional shortening (FS) in mice ($n=6$). (**F**–**H**) Measurement of left ventricular internal dimension at diastole (LVID; d), left ventricular internal dimension at systole (LVID; s), and left ventricular anterior wall thickness at diastole (LVAW; d) in mice ($n=6$). (**I**) Intraperitoneal glucose tolerance test in mice of four groups at 15 min, 30 min, 60 min, 90 min and 120 min. (**J**) Area under curve (AUC) of intraperitoneal glucose tolerance test. (**K**–**L**) mRNA levels of *ANP* and *BNP* relative to *β-actin* ($n=6$). (**M**) Representative H&E of myocardial cross-sections ($n=6$). Scale bar for upper panel (500 μm), for lower panel (100 μm). (**N**) Representative WGA staining of cardiomyocytes ($n=6$). Scale bar, 50 μm. (**O**) Quantification of cardiomyocyte area in four groups. *$P<0.05$; ns, not significant

glutaraldehyde, sectioning, and staining with 2% uranyl acetate and Reynolds lead citrate. Sections were observed under an 80-kV transmission electron microscope (JEM-1230, JOEL, Japan). Mitochondrial size was measured with Image J software.

Measurement of calpain activity

The cleavage of the calpain substrate was measured using a calpain activity assay kit (Abcam, UK) as described in a previous study [24]. Tissue or cell proteins were extracted and concentration was measured by the BCA protein assay kit, followed by sample dilution in 85 μL extraction buffer. Calpain activity was examined with calpain substrate and reaction buffer. Then, absorbance was measured at 400 nm excitation and 505 nm emission wavelengths.

Mitochondrial function detection

To measure mitochondrial membrane potential (MMP), cultured cells were determined with a JC-10 kit (Solarbio, China) and mitochondrial ROS was estimated with MitoSox Red superoxide indicator (Cell Signaling Technology, USA). For ROS detection, frozen tissue sections or cultured cells were stained with 2',7'-Dichlorofluorescin diacetate (DCFH-DA) or dihydroethidium (DHE) (Beyotime, China). Mitochondrial oxygen consumption rate (OCR) was measured using a Seahorse XF24 analyzer (Agilent, USA) according to protocols. H9C2 cells were seeded at 40,000 cells/well on 24-well XFe24 cell culture microplates. OCR value was measured using the Seahorse XF Cell Mitochondrial Stress Test kit.

Intracellular Ca^{2+} entry measurement

The intracellular Ca^{2+} entry was measured as described in the previous study [24]. Briefly, cells were incubated in a transparent 96-well plate for 3 days, and then treated with 2-μM Fura-2-AM (Thermo Fisher Scientific, USA) for 75 min. Intracellular Ca^{2+} signal changes were estimated through the proportion of 340 nm and 380 nm wavelengths.

Western blot analysis

Heart tissues or cultured cells were lysed with RIPA buffer supplemented with phosphatase and protease inhibitors (Beyotime, China). Protein extractions were separated by 10-12% SDS-PAGE and then transferred to PVDF membranes (Millipore, USA). After blocking with 5% skim milk or BSA for 1 h at room temperature, the membranes were incubated with primary antibodies (all the primary antibodies were shown in Supplementary file 3: Table S3) at 4 °C overnight. Next day, the membranes were washed and incubated with peroxidase-conjugated anti-rabbit IgG (1:5000 dilution, ZSGB-BIO, Beijing, China) and anti-mouse-IgG (1:5000 dilution, ZSGB-BIO, Beijing, China) for 1 h and bands were detected with the ECL detection kit (Epizyme, China). GAPDH or β-actin was used as control indicated in figures. Protein quantification was analyzed with Image J software.

Biochemical analysis

Serum lipid levels, including total cholesterol (TC), triglyceride (TG), low-density lipoprotein cholesterol (LDL-C) and high-density lipoprotein cholesterol (HDL-C) were measured using an automatic biochemical analyzer (URIT-8026, China).

Data collection and RNA-seq analysis

RNA-seq data (GSE241166) from heart tissues of DCM and control mice, generated using the Illumina NovaSeq 6000 platform, was obtained from the Gene Expression Omnibus (GEO) database (https://www.ncbi.nlm.nih.gov/geo/). The dataset included heart samples from three DCM mice (T2DM, induced by HFD and STZ) and three normal mice. To identify differentially expressed genes associated with ion channels, RNA-seq analysis was conducted with a cutoff criterion of fold change more than 1.5 or less than 1/1.5 combined with $P<0.05$.

Statistical analysis

All data were presented as mean ± SEM. For comparisons between two groups, unpaired Student's *t*-test was conducted and for more than two groups, one-way ANOVA followed by Turkey's post hoc test was performed. All statistical tests were conducted using GraphPad Prism software. *P* value less than 0.05 was considered as statistically significant.

Results

Elevation in Piezo1 expression in DCM and HG-treated cells

Previous studies have indicated the up-regulation of Piezo1 in cardiomyocytes of mice with cardiac hypertrophy [25] and ischaemia/reperfusion injury [26]. To

determine whether Piezo1 expression is increased in DCM hearts compared to normal tissues, we downloaded RNA-seq data from the GEO dataset and compared the expression levels of ion channels genes, including Piezo1. The results revealed a significant up-regulation of Piezo1 in DCM samples relative to normal hearts (Fig. 1A, B). To further confirm these findings, *Piezo1*$^{dtT/dtT}$ mice were applied to conduct T2DM and T1DM model. IF staining of heart sections indicated higher protein levels of Piezo1 in T2DM (Fig. 1C, D) and T1DM (Fig. 1E, F) mice. Similarly, H9C2 cells were treated with high glucose (HG, 35 mM), showing increased Piezo1 expression compared to normal glucose (NG, 1 g/L) conditions (Fig. 1G, H). Meanwhile, the results of western blot also presented higher Piezo1 level in HG-treated cells than NG group (Fig. 1I, J). These data underscore the notable increase in Piezo1 expression in DCM mice and HG-treated cells.

Cardiac-specific knockout of Piezo1 improves cardiac function and remodeling

To investigate the role of Piezo1 in diabetic hearts, we constructed *Piezo1*$^{\Delta Myh6}$ mice. The deletion of Piezo1 was confirmed by genotyping (Supplementary file1: Fig. S1A). After Piezo1 deletion, there were no significant differences in the shape, body weight, or organ weight relative to body weight (heart, kidney, liver, lung, or spleen) between *Piezo1*$^{\Delta Myh6}$ and *Piezo1*$^{fl/fl}$ mice (Supplementary file 1: Fig. S1B–D). Moreover, serum levels of TC, TG and glucose did no differ between the two groups (Supplementary file 1: Fig. S1E–G). Piezo1 deletion also showed no significant effect on cardiac function, including EF and FS (Supplementary file 1: Fig. S1H–K). RT-PCR and IF staining of cardiac tissue showed Piezo1 expression was reduced in *Piezo1*$^{\Delta Myh6}$ mice compared to *Piezo1*$^{fl/fl}$ mice (Supplementary file 1: Fig. S1L–N). Calcium imaging also showed an obvious reduction in calcium influx in NMCRs isolated from *Piezo1*$^{\Delta Myh6}$ mice in response to Yoda1 (Supplementary file 1: Fig. S1O, P). Further, we also validated Piezo1 deletion using western blot, and it showed that the level of Piezo1 was decreased in *Piezo1*$^{\Delta Myh6}$ mice (Supplementary file 1: Fig. S1Q, R). These results demonstrated successful cardiac-specific knockout of Piezo1 in *Piezo1*$^{\Delta Myh6}$ mice.

To explore the effect of Piezo1 knockout on cardiac function, echocardiographic analysis was applied. Compared to *Piezo1*$^{fl/fl}$ control mice, those in the *Piezo1*$^{fl/fl}$ + HFD group displayed cardiac dysfunction, as indicated by increased heart weight and decreased LVEF, LVFS, as well as elevated LVID, d, LVID, s and LVPW (Fig. 2B–H). Obviously, these echocardiographic results were all reversed following Piezo1 deletion. Glucose tolerance testing indicated that mice in DCM group exhibited impaired glucose tolerance (Fig. 2I, J). However, there was no difference between *Piezo1*$^{fl/fl}$ and *Piezo1*$^{\Delta Myh6}$ mice. Additionally, serum levels of TC, TG and LDL-C were significantly elevated in *Piezo1*$^{fl/fl}$ + HFD group relative to controls, but were normalized following Piezo1 deletion (Supplementary file 2: Fig. S2A–C). Although serum levels of HDL-C were lower in *Piezo1*$^{fl/fl}$ + HFD group, there was no obvious difference compared to *Piezo1*$^{\Delta Myh6}$ + HFD (Supplementary file 2: Fig. S2D).

Natriuretic peptides including atrial natriuretic peptide (ANP) and brain natriuretic peptide (BNP) have been considered as cardioprotective factors. RT-PCR results showed that the levels of *ANP* and *BNP* were significantly elevated in *Piezo1*$^{fl/fl}$ + HFD group, while these effects were attenuated by *Piezo1* knockout, indicating cardiac injury was partially repaired (Fig. 2K, L). Myocardial disarray was markedly evident in the *Piezo1*$^{fl/fl}$ + HFD group compared to control mice, yet this abnormality was restored upon Piezo1 deletion (Fig. 2M). Furthermore, WGA staining revealed significantly smaller cross-sectional area of cardiomyocytes in *Piezo1*$^{\Delta Myh6}$ + HFD mice relative to those in the *Piezo1*$^{fl/fl}$ + HFD group (Fig. 2N, O). Collectively, these results indicate that Piezo1 deletion ameliorates cardiac dysfunction.

Alleviation of cardiac fibrosis with Piezo1 deficiency

Given that cardiac fibrosis is a prominent feature of DCM, we detected the extent of myocardial fibrosis through Masson's trichrome staining. Increased collagen accumulation within the prevascular and interstitial region was observed in *Piezo1*$^{fl/fl}$ + HFD mice compared to *Piezo1*$^{\Delta Myh6}$ + HFD counterparts (Fig. 3A–C). IF staining for collagen I and collagen III also exhibited higher collagen levels in *Piezo1*$^{fl/fl}$ + HFD than in the in *Piezo1*$^{\Delta Myh6}$ + HFD group (Fig. 3D–F). These findings indicate that cardiac-specific Piezo1 deficiency alleviated cardiac fibrosis in DCM hearts.

Impaired oxidative stress and mitochondrial dysfunction reversed due to Piezo1 deficiency

Considering the pivotal role of oxidative stress and mitochondria dysfunction in DCM development, we evaluated ROS levels across all groups using DHE and DCFH-DA probes in cardiac tissues. The results revealed elevated fluorescence intensities in the tissues of *Piezo1*$^{fl/fl}$ + HFD mice compared to control mice, which reduced after Piezo1 knockout in cardiac tissues (Fig. 4A–C). Mitochondria-derived anions are known as the principal intracellular source of ROS in DCM. Moreover, increased mitochondria fragmentation is a key feature of diabetes, suggesting a role for abnormal fission in ROS production and mitochondrial dysfunction [27, 28]. Therefore, TEM analysis was conducted to examine the mitochondrial morphology and function. Findings showed abnormal density, disordered arrangements and fragmentation of mitochondria in the *Piezo1*$^{fl/fl}$ + HFD group, with Piezo1

deficiency ameliorating these alterations (Fig. 4D). Additionally, Piezo1 knockout reversed mitochondrial length and morphology compared with *Piezo1*$^{fl/fl}$ + HFD mice (Fig. 4E). Collectively, these results indicate that cardiac-specific Piezo1 knockout significantly improves diabetes-induced mitochondrial dysfunction.

Enhanced mitochondrial function in vitro with Piezo1 deficiency

To mimic hyperglycemic and hyperlipidemia environment in vivo, H9C2 cells and NMCMs were treated with high glucose in combination with palmitate (HG + PA). The results showed that HG + PA treated cells exhibited elevated ROS levels (Fig. 5A, B and D, E). To further delineate the effect of Piezo1 on MMP, the JC-10 fluorescent probe was applied. The MMP level was reflected by the ratio of green to red fluorescence, with data showing that aggregates probes were markedly reduced but monomers increased following HG + PA treatment (Fig. 5C, F). Interestingly, the application of GsMTx4, a Piezo1 inhibitor, markedly reversed changes in ROS and MMP levels.

To examine the role of Piezo1 in mitochondrial function in more depth, NMCMs were isolated from *Piezo1*$^{fl/fl}$ and *Piezo1*$^{\Delta Myh6}$ mice, and then subjected to HG + PA treatment. Meanwhile, heightened levels of cell ROS, mitochondrial ROS and monomers were detected in HG + PA treated primary NMCMs, which were reversed by Piezo1 knockout (Fig. 5G–L). Additionally, the Cell Mitochondrial Stress Test analysis indicated that HG + PA treatment also led to decreased maximal respiration and spare capacity, while GsMTx4 treatment reversed these effect (Fig. 5M–O). These data support the contention that Piezo1 deficiency preserves mitochondrial function in HG + PA treated cardiomyocytes.

Regulation of mitochondrial dynamics proteins by Piezo1 through calpain/ERK1/2

Several reports demonstrate that impaired mitochondrial dynamics are detrimental to cardiac health, including DCM [29]. In diabetic hearts of mice in the *Piezo1*$^{fl/fl}$ + HFD group, gene expression related to mitochondrial fission, including *Drp1* and *Fis1*, was significantly increased compared to the control mice, whereas expression of genes associated with mitochondrial fusion, including *MFN1*, *MFN2* was reduced (Fig. 6A–D). Piezo1 knockout significantly reversed their mRNA levels. H9C2 cells stained with Tomm20 and DAPI demonstrated that HG + PA treatment led to mitochondrial fragmented compared to low glucose conditions, with GsMTx4 reversing this effect (Fig. 6E, F). IF staining highlighted an increase in phosphorylated Drp1 expression while OPA1 levels were downregulated (Fig. 6G–I), indicating that Piezo1 inhibition protects against HG + PA induced mitochondria dysfunction.

Previous study has shown decreased calpain activity following Piezo1 deficiency in macrophage and endothelial cells [9, 24]. Indeed, our results confirmed that calpain activity was significantly higher in DCM hearts but markedly reduced following Piezo1 deficiency (Fig. 6J). Moreover, elevated calpain activity in HG + PA induced cells was also reversed after GsMTx4 treatment or Piezo1 knockout (Fig. 6K, L). Collectively, these data demonstrate that Piezo1 regulates calpain activity during the progression of DCM.

Furthermore, we validated protein levels associated with mitochondria dynamics using WB analysis. In diabetic hearts, OPA1 was remarkably reduced in *Piezo1*$^{fl/fl}$ + HFD compared to controls. In contrast, levels of p-Drp1 at ser616 not at ser637 were significantly increased in diabetic hearts, although the levels of total Drp1 remained unchanged. Particularly, ERK1/2 is known to phosphorylate Drp1 at ser616, which triggers abnormal mitochondrial fission in cardiac injury [30, 31]. Our data revealed that *Piezo1*$^{fl/fl}$ + HFD mice exhibited elevated levels of p-ERK1/2group, while total ERK1/2 levels did not change. Piezo1 deficiency led to a significant increase in OPA1 and decreases in p-Drp at ser616 and p-ERK1/2 levels (Fig. 7A–G). In H9C2 cells and NMCMs, HG + PA treatment also resulted in upregulated p-Drp1 at ser616 and p-ERK1/2 without affecting total protein levels (Fig. 7H–Q). Interestingly, both Piezo1 inhibitor and deletion reversed this effect. Altogether, these data indicates that Piezo1 regulates mitochondria dynamics via ERK1/2-mediated phosphorylation.

Aggravation of cardiac remodeling by Piezo1 activation

To further confirm the physiological role of Piezo1 in DCM development and heart failure in vivo, we evaluated the effects of Piezo1 agonist, Yoda1 upon DCM in C57JL/6 mice. For this purpose, we administrated Yoda1 (i.p injection) to mice after 12 weeks for STZ injection (Fig. 8A). We then examined cardiac function by echocardiography and discovered that STZ induced obvious LV systolic dysfunction, which was aggravated by Yoda1 administration, as identified by decreased LVEF and LVFS, and increased heart mass (Fig. 8B–D). Likewise, Yoda1 treatment enhanced collagen deposition relative to the STZ-induced DCM heart (Fig. 8E–G). Increased levels of *ANP* and *BNP* were obviously increased after Yoda1 injection (Fig. 8H, I). IF staining showed a significant increase of collagen I and III in mice administrated with Yoda1 compared to those in the DCM group (Fig. 8J–L). This striking correlation of Yoda1 and DCM underscores the critical role of Piezo1 in the progression of this disease.

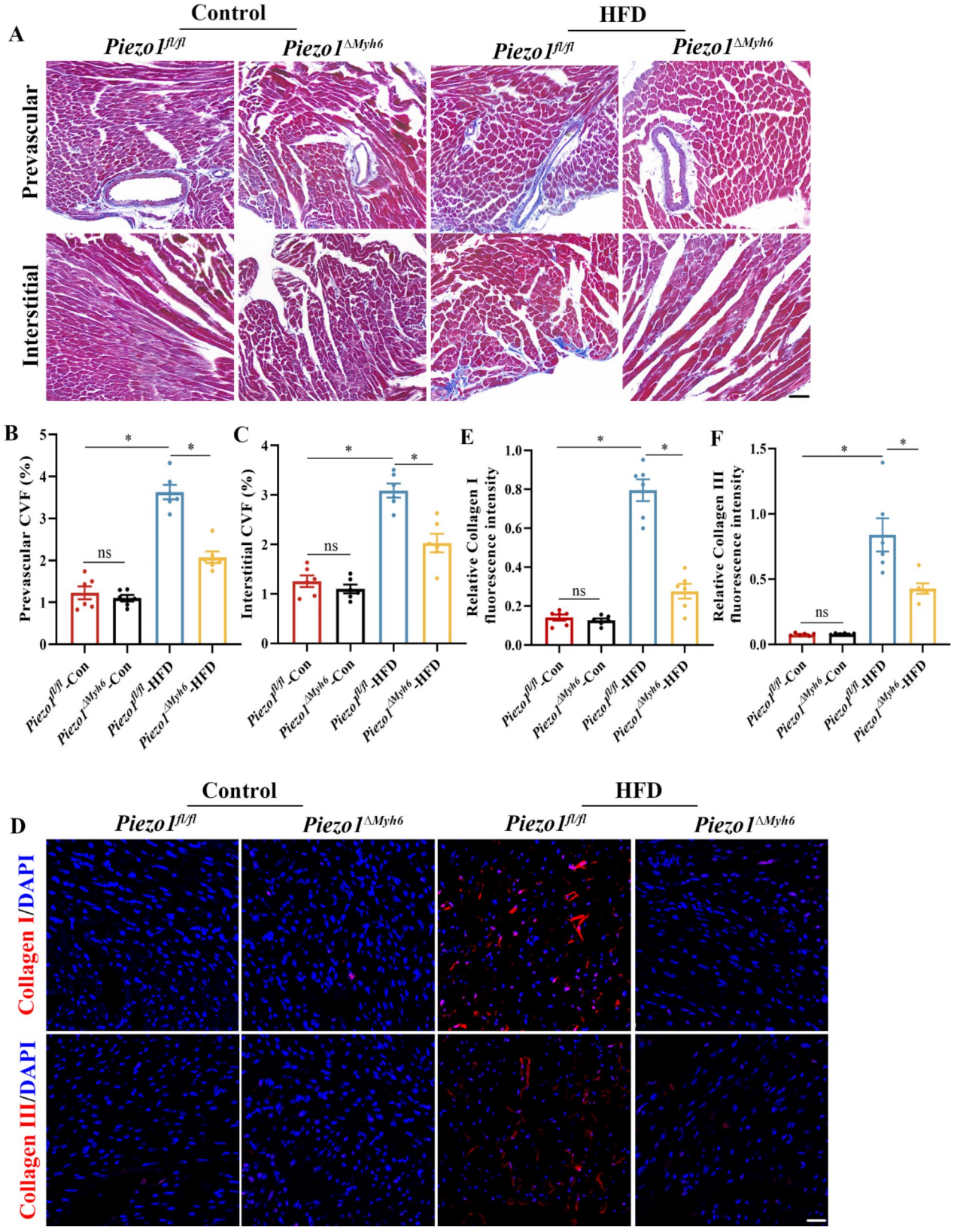

Fig. 3 Piezo1 deficiency alleviated cardiac fibrosis induced by diabetes in vivo. (**A**) Representative images of Masson's trichrome staining of hearts in four groups of mice ($n=6$). Scale bar, 50 μm (**B**, **C**) Quantification of perivascular and interstitial collagen volume fraction (CVF) in four groups of mice. (**D**) Immunofluorescence of collagen I and collagen III in four groups of mice ($n=6$). Scale bar, 50 μm (**E**, **F**) Quantification of immunofluorescence of collagen I and collagen III. *$P<0.05$; ns, not significant

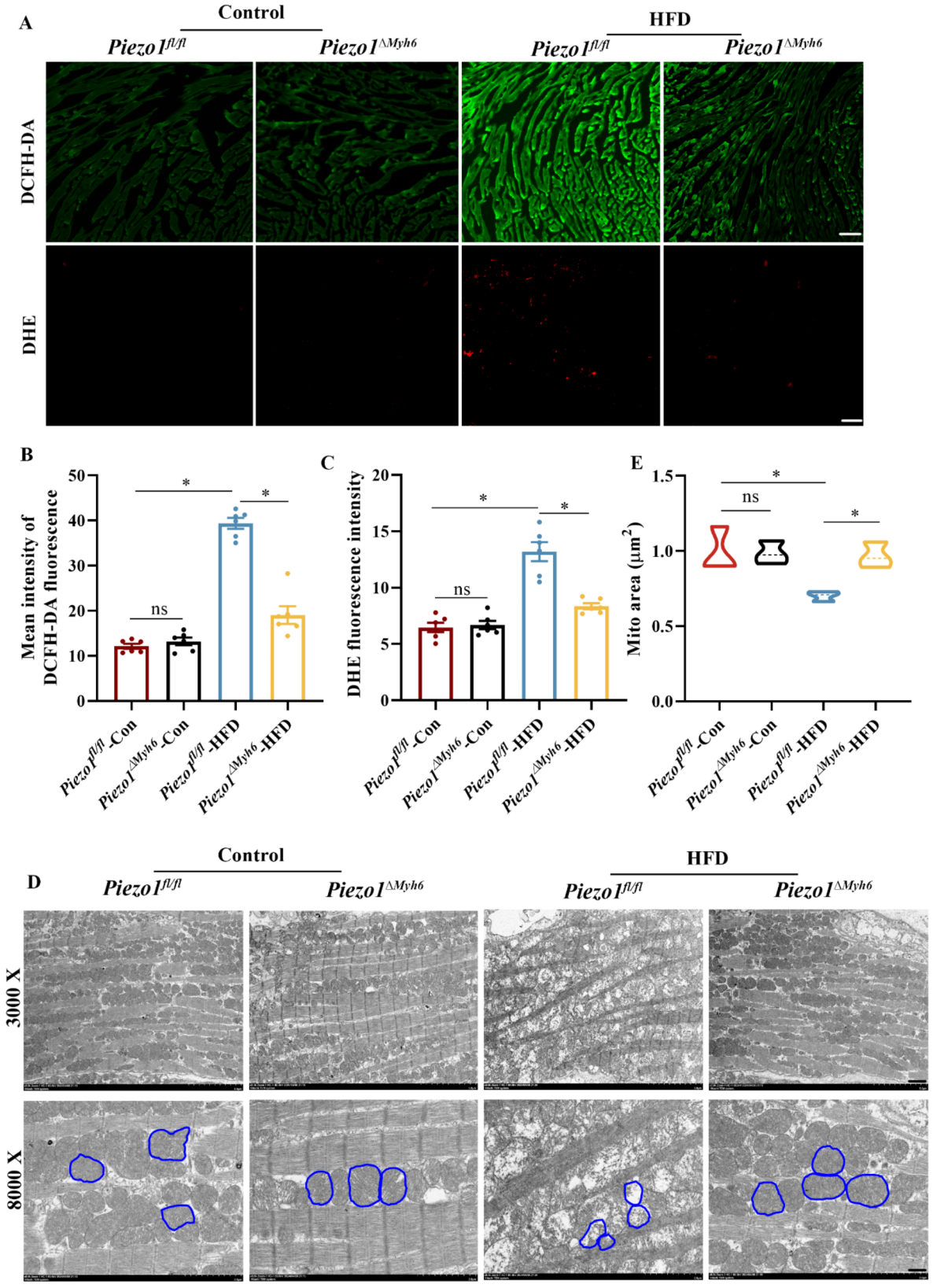

Fig. 4 Piezo1 prevents mitochondrial ROS production and dysfunction in the hearts of diabetic mice. (**A**) Representative images of DCFH-DA and DHE staining of the cardiac tissues ($n=6$). (**B**, **C**) Quantification of fluorescence intensity in A. (**D**) Representative images of mitochondrial ultrastructure with TEM in myocardial tissues from four groups ($n=6$). Scale bar for the upper panel, 0.5 μm; scale bar for the lower panel, 0.2 μm. (**E**) Quantification of mitochondrial area in D. *$P<0.05$; ns, not significant

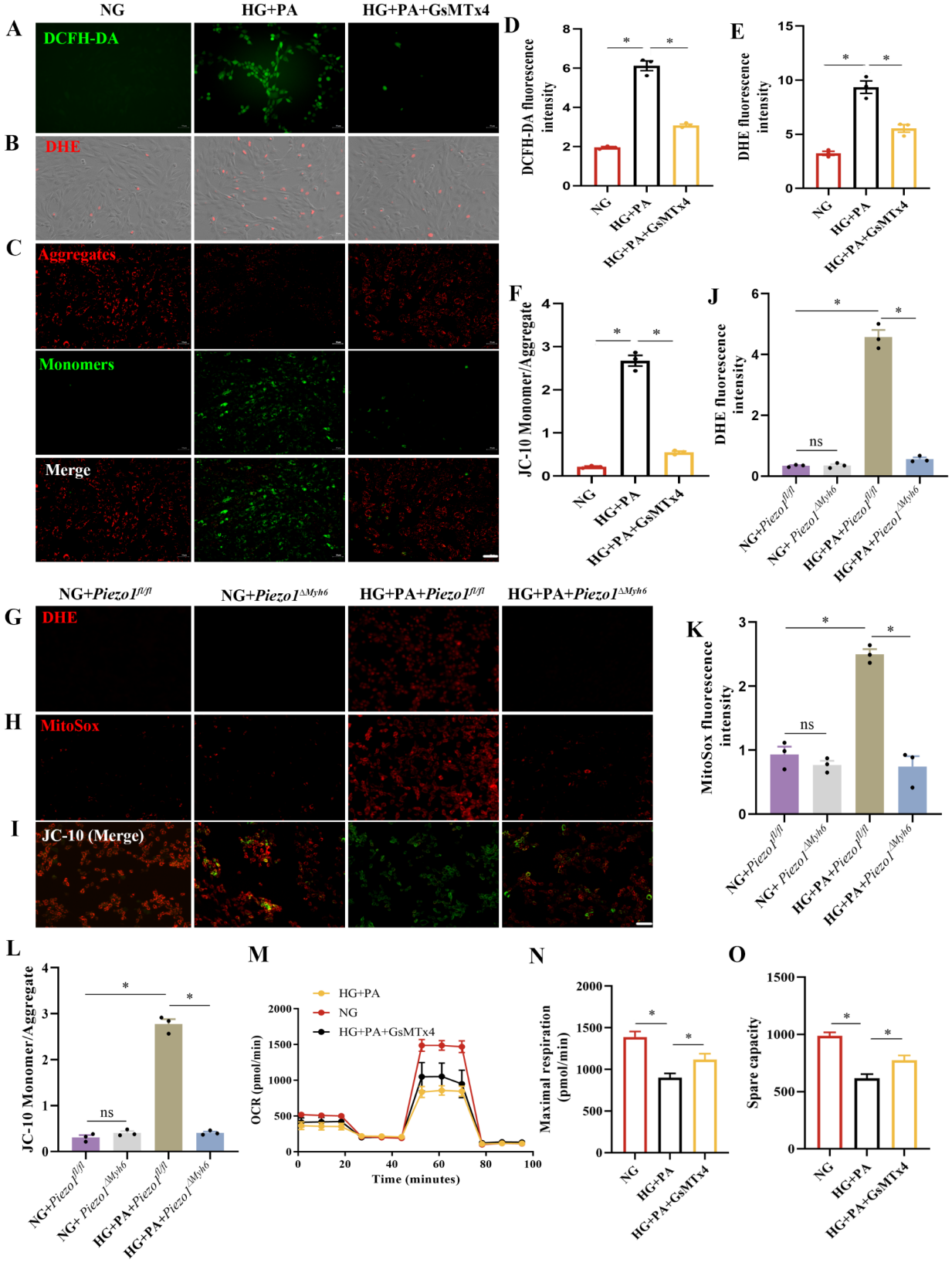

Fig. 5 (See legend on next page.)

(See figure on previous page.)

Fig. 5 Piezo1 inhibition attenuates mitochondrial function in cardiomyocytes. H9C2 cells or NMCMs were treated high glucose and palmitate (HG + PA), and then H9C2 cells were treated with GsMTx4. (**A**–**F**) Representative images of DCFH-DA (**A**), DHE (**B**), and JC-10 (**C**) staining and corresponding quantitative analysis of fluorescence intensity in GsMTx4-treated H9C2 cells ($n = 3$). (**G**–**L**) Representative images of DHE (**G**), MitoSox (**H**), and JC-10 (**I**) staining and corresponding quantitative analysis of fluorescence intensity in NMCMs ($n = 3$). (**M**–**O**) Mitochondrial respiration function in GsMTx4-treated H9C2 cells was assessed by OCR assay. $^*P < 0.05$; ns, not significant

Discussion

Ample epidemiological evidence has documented a strong correlation between diabetes and heart failure [32, 33]. Patients with diabetes often experience myocardial dysfunction, characterized by myocardial fibrosis, cardiac remodeling, diastolic and systolic dysfunction [34]. This condition is termed as DCM and increasing molecular targets for DCM treatment have been found [35, 36]. Emerging studies have focused on the role of Piezo1 in cardiovascular pathophysiology, including myocardial infarction [10], atherosclerosis [37] and lymphatic development [38]. Our findings provide several interesting insights. First, we observed a significant increase in Piezo1 expression in the hearts of diabetic mice and in HG-treated cardiomyocytes. Second, cardiac-specific knockout of Piezo1 improved cardiac dysfunction and remodeling, thereby mitigating myocardial fibrosis. Third, Piezo1 deletion alleviated cardiac dysfunction by restoring mitochondrial fragmentation and altering MMP, both in vivo and in vitro, via the ERK/Drp1 signaling pathway. Lastly, Piezo1 activation aggravated cardiac damage through increased collagen synthesis. To the best of our knowledge, this study presents the first report demonstrating the important role of Piezo1 in the progression of DCM and the potential underlying mechanisms involved.

Mechanically, cardiac hypertrophy develops in response to increased workload. While our present study elucidates the vital roles of Piezo1 in diabetes and heart dysfunction, the specific regulatory mechanisms of Piezo1 in diabetes complications like DCM require further exploration. The pathophysiology of DCM is complex. Importantly, approximately 95% of ATP is generated by cardiac muscle originating from oxidative phosphorylation in mitochondria, suggesting the key role of mitochondrial dysfunction is DCM progression. Mitochondria possess active Ca^{2+} transport systems and several enzymes related to energy metabolism are activated by Ca^{2+}. ROS overload is considered as a key trigger of oxidative stress which is one obvious characteristic of DCM. The present study supported the role of oxidative stress in controlling DCM progression in vivo and in vitro. ROS levels were increased in diabetic hearts and HG + PA treated cells but reduced after Piezo1 deletion or inhibitor treatment. Moreover, lipid metabolism plays a vital role in diverse physiological process of heart and cardiovascular diseases. Importantly, lipotoxicity could induce endoplasmic reticulum stress, cell death, inflammatory responses and mitochondrial dysfunction [39]. We also found increased serum levels of total cholesterol (TC), triglycerides (TG), and low-density lipoprotein cholesterol (LDL-C) in the $Piezo1^{fl/fl}$ + HFD group but reversed after Piezo1 deletion. Additionally, mitochondrial dysfunction is related to several mechanisms in the pathogenesis of DCM, including mitochondrial morphology, integrity, dynamics, mitophagy and biogenesis [17]. Mitochondrial dynamics, including mitochondrial fission and fusion could regulate mitochondrial size, mass and intercellular lipid accumulation [40]. Emerging evidence has shown that the imbalance of mitochondrial fission and fusion plays a vital role in the diabetic heart [41–43]. In diabetic patients and mice, Drp1 was significantly upregulated whereas OPA1 was downregulated, which was consistent with our results [44, 45]. Interestingly, cardiomyocyte-specific knockout of Piezo1 improved mitochondrial function through inhibiting mitochondrial fragmentation and fission, and suppressing oxidative stress.

Calpain can be activated by high level of Ca^{2+} and widely expressed in eukaryotic cells [46]. We hypothesized that calpain is involved in HFD/STZ induced heart failure via Piezo1 activation induced Ca^{2+} entry. Previous data from our team has shown that calpain is acting downstream of Piezo1. Meanwhile, HG-induced upregulation of calpain1 expression has been reported in H9C2 cells, which was consistent with our results [47]. We also found HG + PA treatment increases mitochondrial fission but decreases mitochondrial fusion. Interestingly, inhibition of calpain activity could dephosphorylate Drp1 at ser637 and suppress mitochondrial fission in acute viral myocarditis [48]. These data together indicate that Piezo1 induced calpain activity regulates mitochondrial dynamics.

As a key component for mitochondrial fission, post-translational modifications to Drp1, such as SUMOylation, phosphorylation and S-nitrosylation are crucial for fission activity [49–51]. In this study, we demonstrated that ERK1/2-mediated $Drp1^{ser616}$ phosphorylation regulated mitochondrial dynamics in the development of diabetic hearts. ERK1/2 is a member of the mitogen active protease (MAPK) family, which promotes cell division and proliferation [52]. A number of reports have indicated that Drp1 is phosphorylated by ERK1/2 at serine 616 site, leading to aberrant mitochondrial fission [53, 54]. Our study showed that Piezo1 inhibitor, GsMTx4 obviously inhibited HG + PA induced

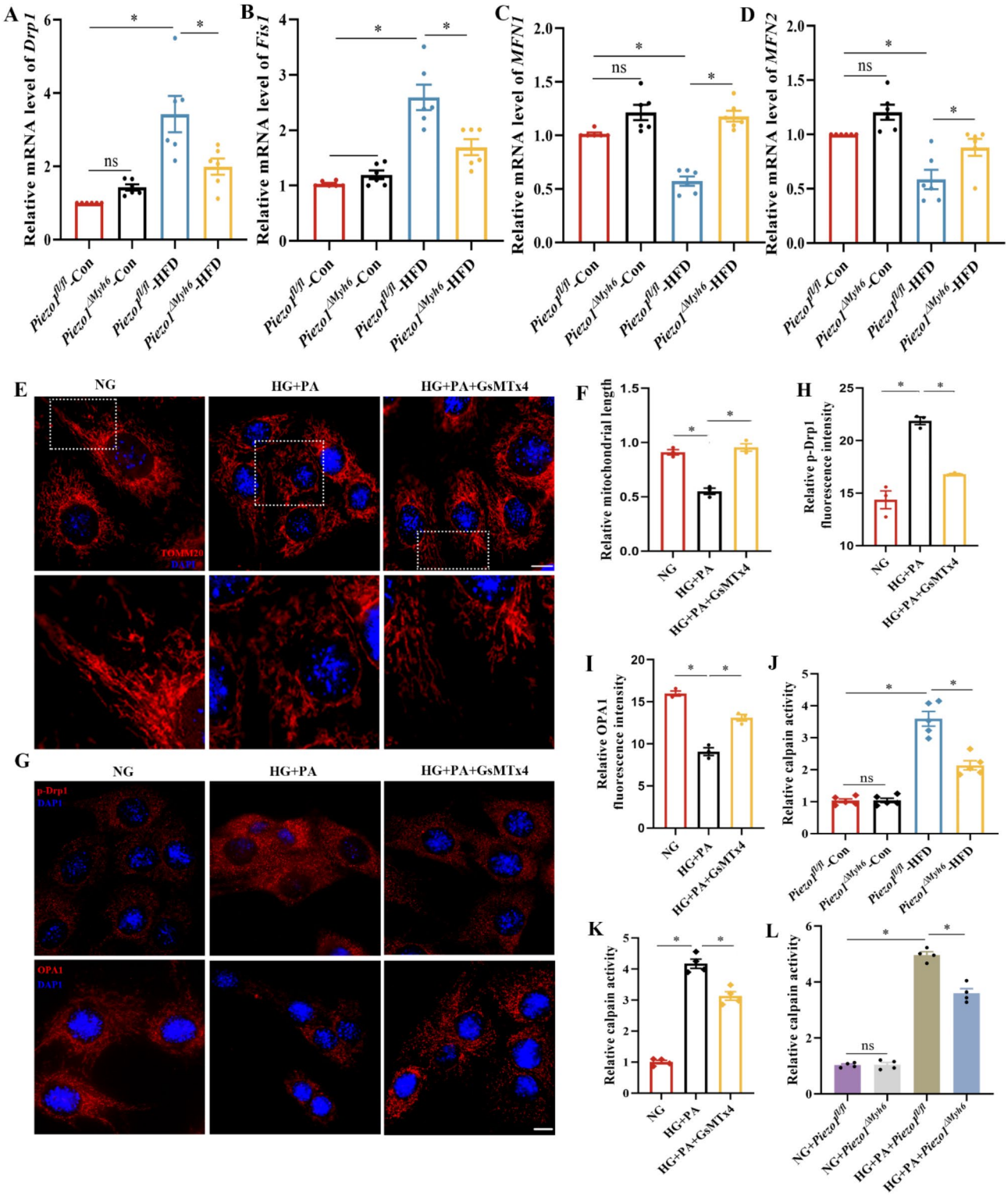

Fig. 6 Piezo1 inhibition regulates mitochondrial fission and fusion via regulating calpain activity. (**A**–**D**) Relative mRNA levels of mitochondrial dynamics-related genes in mouse hearts ($n=6$). β-actin was used as internal control. (**E**, **F**) Representative fluorescence images of TOMM20 and DAPI in H9C2 cells and quantification of mitochondrial length. (**G**–**I**) Representative fluorescence images of phos(Ser616)-Drp1 and OPA1 in H9C2 cells corresponding quantification ($n=3$). (**J**–**L**) Measurements of calpain activity in heart tissues from mice, H9C2 cells and NMCMs ($n=4$). *$P<0.05$; ns, not significant

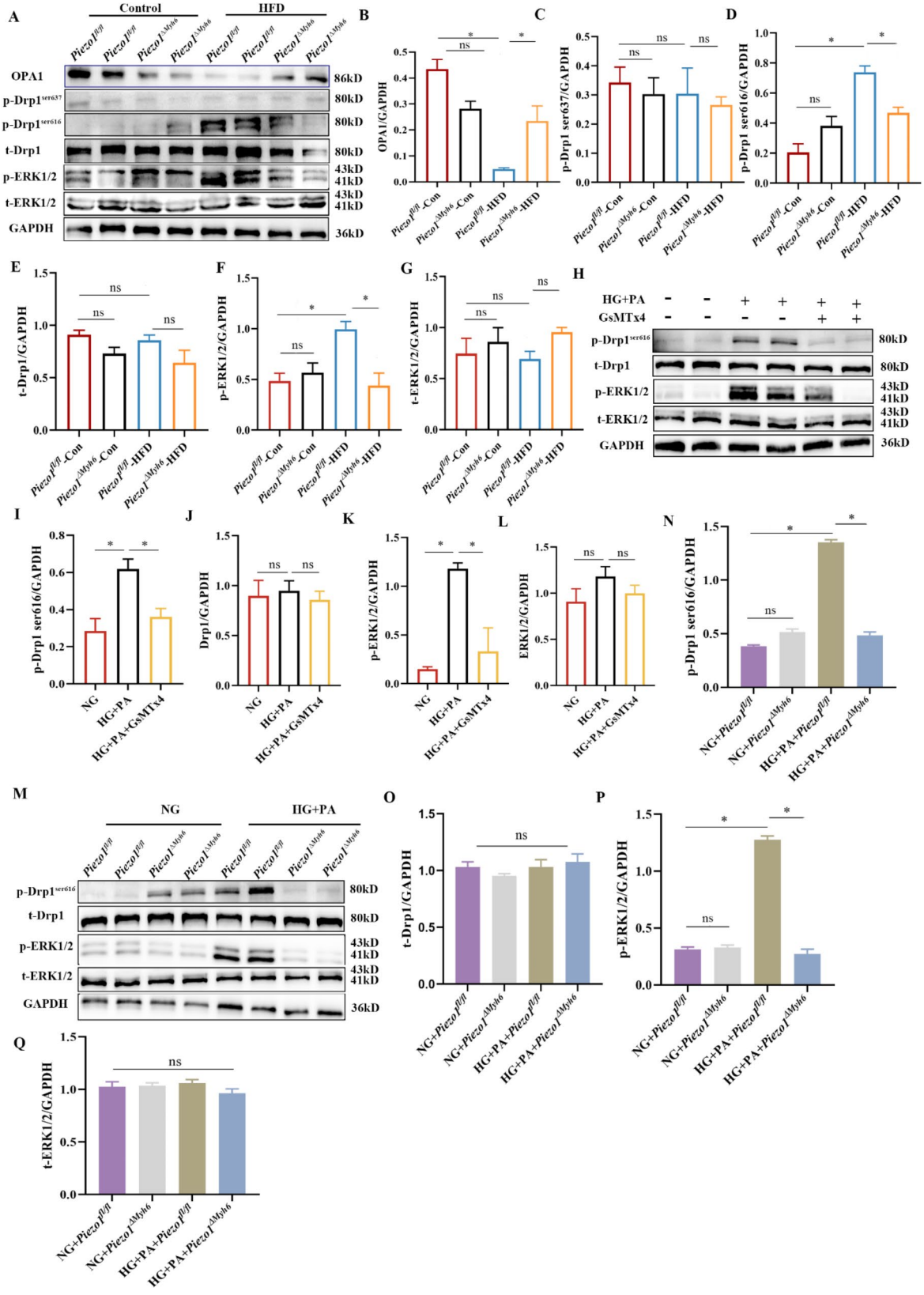

Fig. 7 Piezo1 regulates mitochondrial dynamics in DCM through Drp1/ERK1/2. (**A**–**G**) Representative immunoblot and quantification of OPA1, phos(Ser637)-Drp1, phos(Ser616)-Drp1, Drp1, phos-ERK1/2 and ERK1/2 in myocardial tissues, normalized to GAPDH. (**H**–**L**) Representative immunoblot and quantification of phos(Ser616)-Drp1, Drp1, phos-ERK1/2 and ERK1/2 in H9C2 cells, normalized to GAPDH. (**M**–**Q**) Representative immunoblot and quantification of phos(Ser616)-Drp1, Drp1, phos-ERK1/2 and ERK1/2 in NMCMs, normalized to GAPDH. $n = 3$. $^{*}P < 0.05$; ns, not significant

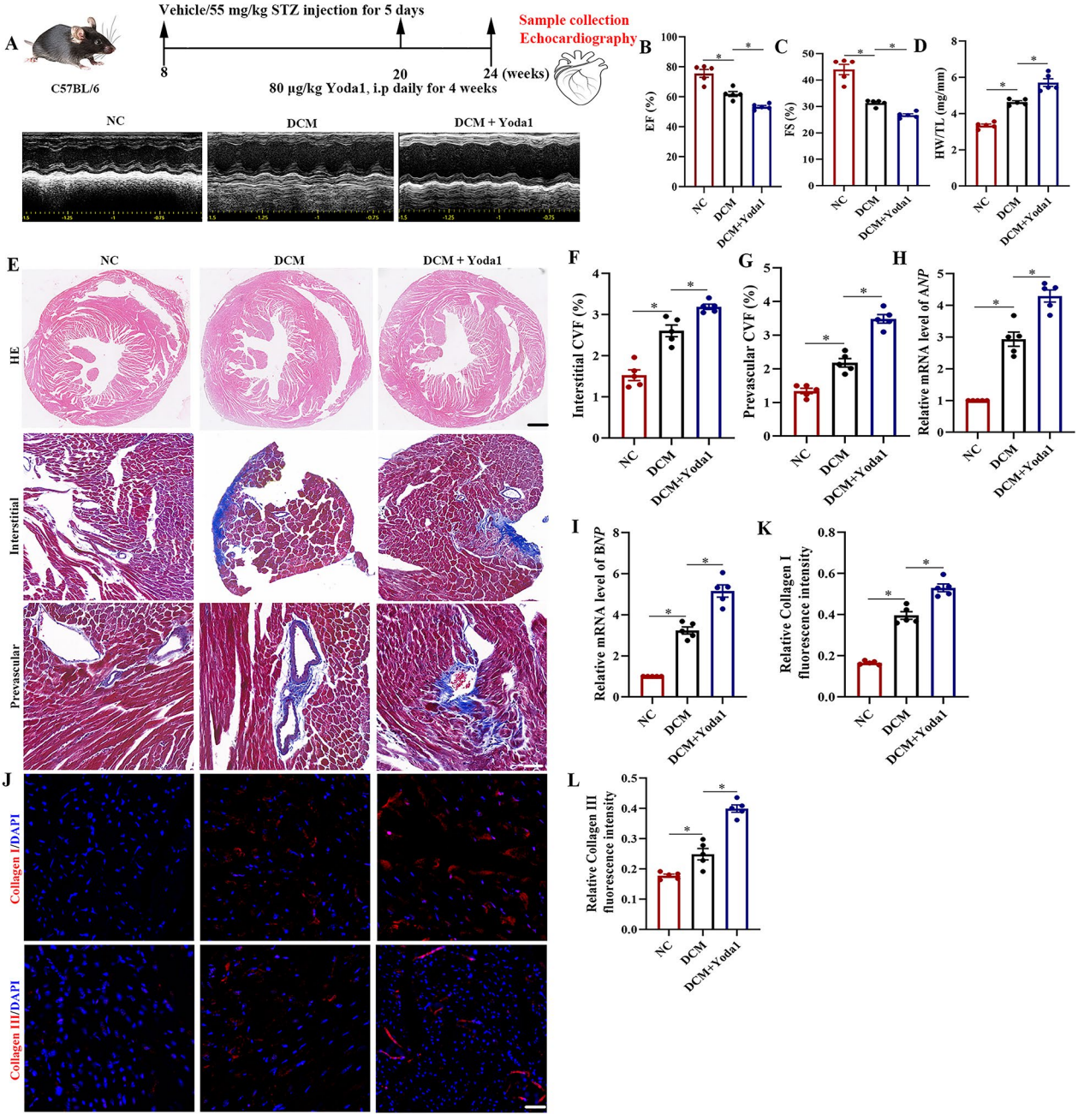

Fig. 8 Cardiac activation of Piezo1 aggravated left ventricular function and remodeling in diabetic mice. (**A**) Experiment timeline and echocardiographic images showing cardiac function of mice in three groups. (**B**–**C**) Quantitative analysis of EF and FS ($n = 5$). (**D**) Quantification of the ratio of heart weight (HW) to tibial length (TL) in three groups of mice ($n = 5$). (**E**–**G**) Representative H&E and Masson's trichrome staining, and quantification of perivascular and interstitial collagen volume fraction (CVF) of myocardial cross-sections in three groups of mice ($n = 5$). (**H**, **I**) Relative mRNA levels of *ANP* and *BNP* in mouse hearts ($n = 5$). β-actin was used as internal control. (**J**–**L**) Immunofluorescence and quantification of collagen I and collagen III in three groups of mice ($n = 5$). Scale bar, 50 μm. $^*P < 0.05$

oxidative stress and mitochondrial fission via downregulating phosphorylation of ERK1/2 and Drp1 at ser616.

In the present study, there are several limitations. First, complicated mechanisms may be involved in DCM including inflammation, impaired insulin sensitivity, altered cardiac metabolic pathway (chronic hyperglycemia, lipotoxicity and dyslipidemia) and mitochondrial mitophagy other than mitochondrial dynamics [27]. In addition, considering the importance of mitochondrial proteins in mitochondrial dynamics, other proteins possibly contributing to DCM progression and in-depth study on association between calpain and p-ERK1/2 deserve further scrutiny. Second, we focus mainly on type 2 diabetes induced DCM, but whether Piezo1 regulates

mitochondrial dynamics in type 1 diabetic heart needs further investigation. Finally, although Piezo1 agonist, Yoda1 is used to activate the ion channel in our study, Yoda1 may activate Piezo1 in immune cells, endothelial cells and epithelial cells other than cardiomyocytes. Therefore, to delineate its unique role in DCM, a cardiac-specific Piezo1 overexpression mouse model would be urgently required.

In conclusion, Piezo1 expression was increased in DCM and cardiac-specific knockout of Piezo1 attenuated cardiac fibrosis and improved cardiac function. Piezo1 deficiency or channel closing decreased calpain levels and phosphorylated Drp1 induced mitochondrial fragmentation by downregulating ERK1/2 phosphorylation (Graphical Abstract). Thus, inhibition of Piezo1 by drug treatment or cardiac-specific gene provides a promising approach to the clinical application for DCM treatment.

Abbreviations

TIDM	Type 1 diabetes
T2DM	Type 2 diabetes
DCM	Diabetic cardiomyopathy
LVEF	Left ventricular ejection fraction
LVFS	Left ventricular shortening fraction
LVID;d	Left ventricular internal dimension at diastole
LVID;s	Left ventricular internal dimension at systole
LVAW;d	Left ventricular anterior wall thickness at diastole
LVAW;s	Left ventricular anterior wall thickness at systole
LVPW;d	Left ventricular posterior wall thickness at diastole
LVPW;s LV	Left ventricular posterior wall thickness at systole

Supplementary Information

The online version contains supplementary material available at https://doi.org/10.1186/s12933-025-02625-8.

Supplementary Material 1: Figure S1. Piezo1 knockout not affect normal heart function. (**A**) Representative genotyping results for Piezo1$^{fl/fl}$ and Piezo1$^{\Delta Myh6}$ mice. (**B**) Body weight of Piezo1$^{fl/fl}$ and Piezo1$^{\Delta Myh6}$ mice. (**C**) The body shape of Piezo1$^{fl/fl}$ and Piezo1$^{\Delta Myh6}$ mice. (**D**) Weight of each organ relative to body weight in Piezo1$^{fl/fl}$ and Piezo1Δ*Myh6* mice. (**E**–**G**) The serum levels of total cholesterol (TC), total triglycerides (TG) and glucose of Piezo1$^{fl/fl}$ and Piezo1$^{\Delta Myh6}$ mice. (**H**–**J**) Representative M-mode echocardiographic images and quantitative measurement of the left ventricle ejection fraction and fractional shortening in Piezo1$^{fl/fl}$ and Piezo1Q mice. (**K**) Electrocardiogram analysis of Piezo1fl/fl and Piezo1$^{\Delta Myh6}$ mice. (**L**) Relative mRNA level of Piezo1 in Piezo1fl/fl and Piezo1$^{\Delta Myh6}$ mice. (**M**, **N**) Immunofluorescent staining and quantitative measurement of Piezo1 in Piezo1$^{fl/fl}$ and Piezo1$^{\Delta Myh6}$ mice. n = 5 per group. (**O**, **P**) Traces showing Ca^{2+} entry and mean data of relative peak value in cardiomyocytes from Piezo1$^{fl/fl}$ and Piezo1$^{\Delta Myh6}$ mice in response to Yoda1 treatment (n = 3). (**Q**, **R**) Western blot and quantitative analysis for Piezo1 in cardiac tissues (n = 3). **P* < 0.05.

Supplementary Material 2: Figure S2. Piezo1 knockout lowers the level of serum lipid in DCM mice. Serum total triglycerides (TG, **A**), total cholesterol (TC, **B**), low-density lipoprotein cholesterol (LDL-C, **C**) and high-density lipoprotein cholesterol (HDL-C, **D**) were assessed in four groups of mice (n = 6). **P* < 0.05; ns, not significant.

Supplementary Material 3

Author contributions

W. Niu designed and performed in vivo and in vitro experiments, data analysis and wrote the manuscript. X. Liu, B. Deng, T. Hong, C. Wang, Y. Yan, and J. Liu participated in data collection and statistical analysis. Y. Jiang provided technical support. J. Li conceptualized and supervised experiments, generated research funds and wrote the manuscript.

Funding

This work was supported by the grants from National Natural Science Foundation of China (Grant Number: 82174196), "20 New Colleges and Universities in Jinan City" (Grant Number: 202228095), Project of National Center for Inheritance and Innovation of Chinese Medicine (Grant Number: 2022ZD05) and Natural Science Joint Foundation of Shandong Province (Grant Number: ZR2022LZY012).

Data availability

No datasets were generated or analysed during the current study.

Declarations

Competing interests

The authors declare no competing interests.

Author details

[1]Innovation Research Institute of Traditional Chinese Medicine, Shandong University of Traditional Chinese Medicine, Jinan 250014, China
[2]Central Laboratory, Shandong University of Traditional Chinese Medicine Affiliated Hospital, Jinan 250014, China
[3]Shandong Institute of Commerce and Technology, Jinan 250103, China
[4]The Second Affiliated Hospital of Guangzhou Medical University, Guangzhou Medical University, Guangzhou 510260, China
[5]Lingnan Medical Research Center, Guangzhou University of Chinese Medicine, Guangzhou 510405, China
[6]The First Affiliated Hospital, Guangzhou University of Chinese Medicine, Guangzhou 510405, China
[7]School of Biomedical Sciences, Faculty of Biological Sciences, University of Leeds, Leeds LS2 9JT, UK

Received: 16 December 2024 / Accepted: 3 February 2025
Published online: 20 March 2025

References

1. Graczyk P, Dach A, Dyrka K, Pawlik A. Pathophysiology and advances in the therapy of cardiomyopathy in patients with diabetes mellitus. Int J Mol Sci. 2024;25(9).
2. Coste B, Mathur J, Schmidt M, Earley TJ, Ranade S, Petrus MJ, et al. Piezo1 and Piezo2 are essential components of distinct mechanically activated cation channels. Science. 2010;330(6000):55–60.
3. Solis AG, Bielecki P, Steach HR, Sharma L, Harman CCD, Yun S, et al. Mechanosensation of cyclical force by PIEZO1 is essential for innate immunity. Nature. 2019;573(7772):69–74.
4. Wang S, Chennupati R, Kaur H, Iring A, Wettschureck N, Offermanns S. Endothelial cation channel PIEZO1 controls blood pressure by mediating flow-induced ATP release. J Clin Invest. 2016;126(12):4527–36.
5. Allison SJ, Hypertension. Mechanosensation by PIEZO1 in blood pressure control. Nat Rev Nephrol. 2017;13(1):3.
6. Segel M, Neumann B, Hill MFE, Weber IP, Viscomi C, Zhao C, et al. Niche stiffness underlies the ageing of central nervous system progenitor cells. Nature. 2019;573(7772):130–4.
7. He L, Si G, Huang J, Samuel ADT, Perrimon N. Mechanical regulation of stem-cell differentiation by the stretch-activated Piezo channel. Nature. 2018;555(7694):103–6.
8. Sugimoto A, Miyazaki A, Kawarabayashi K, Shono M, Akazawa Y, Hasegawa T, et al. Piezo type mechanosensitive ion channel component 1 functions as a regulator of the cell fate determination of mesenchymal stem cells. Sci Rep. 2017;7(1):17696.
9. Li J, Hou B, Tumova S, Muraki K, Bruns A, Ludlow MJ, et al. Piezo1 integration of vascular architecture with physiological force. Nature. 2014;515(7526):279–82.
10. Sun M, Mao S, Wu C, Zhao X, Guo C, Hu J, et al. Piezo1-mediated neurogenic inflammatory cascade exacerbates ventricular remodeling after myocardial infarction. Circulation. 2024;149(19):1516–33.

11. Lim GB. Piezo1 senses pressure overload and initiates cardiac hypertrophy. Nat Rev Cardiol. 2022;19(8):503.
12. Lee W, Leddy HA, Chen Y, Lee SH, Zelenski NA, McNulty AL, et al. Synergy between Piezo1 and Piezo2 channels confers high-strain mechanosensitivity to articular cartilage. Proc Natl Acad Sci USA. 2014;111(47):E5114–22.
13. Niu L, Cheng B, Huang G, Nan K, Han S, Ren H, et al. A positive mechano-biological feedback loop controls bistable switching of cardiac fibroblast phenotype. Cell Discov. 2022;8(1):84.
14. Xiao B. Mechanisms of mechanotransduction and physiological roles of PIEZO channels. Nat Rev Mol Cell Biol. 2024;25(11):886–903.
15. Yu Z, Gong H, Kesteven S, et al. Piezo1 is the cardiac mechanosensor that initiates the cardiomyocyte hypertrophic response to pressure overload in adult mice. Nat Cardiovasc Res. 2022;1:577–91.
16. Ye Y, Barghouth M, Dou H, Luan C, Wang Y, Karagiannopoulos A, et al. A critical role of the mechanosensor PIEZO1 in glucose-induced insulin secretion in pancreatic beta-cells. Nat Commun. 2022;13(1):4237.
17. Chang X, Li Y, Cai C, Wu F, He J, Zhang Y, et al. Mitochondrial quality control mechanisms as molecular targets in diabetic heart. Metabolism. 2022;137:155313.
18. Wang T, Wang X, Fu T, Ma Y, Wang Q, Zhang S, et al. Roles of mitochondrial dynamics and mitophagy in diabetic myocardial microvascular injury. Cell Stress Chaperones. 2023;28(6):675–88.
19. Rovira-Llopis S, Banuls C, Diaz-Morales N, Hernandez-Mijares A, Rocha M, Victor VM. Mitochondrial dynamics in type 2 diabetes: pathophysiological implications. Redox Biol. 2017;11:637–45.
20. Qian Y, Han Q, Zhao X, Song J, Cheng Y, Fang Z, et al. 3D melatonin nerve scaffold reduces oxidative stress and inflammation and increases autophagy in peripheral nerve regeneration. J Pineal Res. 2018;65(4):e12516.
21. Ranade SS, Qiu Z, Woo SH, Hur SS, Murthy SE, Cahalan SM, et al. Piezo1, a mechanically activated ion channel, is required for vascular development in mice. Proc Natl Acad Sci USA. 2014;111(28):10347–52.
22. Tao T, Shu Q, Zhao Y, Guo W, Wang J, Shi Y, et al. Mechanical regulation of lipid and sugar absorption by Piezo1 in enterocytes. Acta Pharm Sin B. 2024;14(8):3576–90.
23. Nicks AM, Holman SR, Chan AY, Tsang M, Young PE, Humphreys DT, et al. Standardised method for cardiomyocyte isolation and purification from individual murine neonatal, infant, and adult hearts. J Mol Cell Cardiol. 2022;170:47–59.
24. He Y, Deng B, Liu S, Luo S, Ning Y, Pan X, et al. Myeloid Piezo1 deletion protects renal fibrosis by restraining macrophage infiltration and activation. Hypertension. 2022;79(5):918–31.
25. Zhang Y, Su SA, Li W, Ma Y, Shen J, Wang Y, et al. Piezo1-mediated mechanotransduction promotes cardiac hypertrophy by impairing calcium homeostasis to activate calpain/calcineurin signaling. Hypertension. 2021;78(3):647–60.
26. Li PB, Bai JQ, Jiang WX, Li HH, Li CM. The mechanosensitive Piezo1 channel exacerbates myocardial ischaemia/reperfusion injury by activating caspase-8-mediated PANoptosis. Int Immunopharmacol. 2024;139:112664.
27. Ritchie RH, Abel ED. Basic mechanisms of diabetic heart disease. Circ Res. 2020;126(11):1501–25.
28. Peterson LR, Gropler RJ. Metabolic and molecular imaging of the diabetic cardiomyopathy. Circ Res. 2020;126(11):1628–45.
29. Rudokas MW, McKay M, Toksoy Z, Eisen JN, Bogner M, Young LH, et al. Mitochondrial network remodeling of the diabetic heart: implications to ischemia related cardiac dysfunction. Cardiovasc Diabetol. 2024;23(1):261.
30. Yu F, Liu F, Luo JY, Zhao Q, Wang HL, Fang BB, et al. Targeted activation of ERK1/2 reduces ischemia and reperfusion injury in hyperglycemic myocardium by improving mitochondrial function. Ann Transl Med. 2022;10(22):1238.
31. Liang X, Wang S, Wang L, Ceylan AF, Ren J, Zhang Y. Mitophagy inhibitor liensinine suppresses doxorubicin-induced cardiotoxicity through inhibition of Drp1-mediated maladaptive mitochondrial fission. Pharmacol Res. 2020;157:104846.
32. Valensi P. Evidence of a bi-directional relationship between heart failure and diabetes: a strategy for the detection of glucose abnormalities and diabetes prevention in patients with heart failure. Cardiovasc Diabetol. 2024;23(1):354.
33. Caturano A, Vetrano E, Galiero R, Sardu C, Rinaldi L, Russo V et al. Advances in the insulin-heart axis: current therapies and future directions. Int J Mol Sci. 2024;25(18).
34. Jia G, Hill MA, Sowers JR. Diabetic cardiomyopathy: an update of mechanisms contributing to this clinical entity. Circul Res. 2018;122(4):624–38.
35. Aroda VR, Taub PR, Stanton AM. Diabetes with cardiomyopathy: at the juncture of knowledge and prevention. J Am Coll Cardiol. 2021;78(16):1599–602.
36. Yao X, Huang X, Chen J, Lin W, Tian J. Roles of non-coding RNA in diabetic cardiomyopathy. Cardiovasc Diabetol. 2024;23(1):227.
37. Pan X, Xu H, Ding Z, Luo S, Li Z, Wan R, et al. Guizhitongluo Tablet inhibits atherosclerosis and foam cell formation through regulating Piezo1/NLRP3 mediated macrophage pyroptosis. Phytomed Int J Phytother Phytopharmacol. 2024;132:155827.
38. Du J, Liu P, Zhou Y, Misener S, Sharma I, Leeaw P et al. The mechanosensory channel PIEZO1 functions upstream of angiopoietin/TIE/FOXO1 signaling in lymphatic development. J Clin Investig. 2024;134(10).
39. Nakamura M. Lipotoxicity as a therapeutic target in obesity and diabetic cardiomyopathy. J Pharm Pharm Sci. 2024;27:12568.
40. Wai T, Langer T. Mitochondrial dynamics and metabolic regulation. Trends Endocrinol Metab. 2016;27(2):105–17.
41. Liu ZY, Lin LC, Liu ZY, Song K, Tu B, Sun H, et al. N(6)-methyladenosine-mediated phase separation suppresses NOTCH1 expression and promotes mitochondrial fission in diabetic cardiac fibrosis. Cardiovasc Diabetol. 2024;23(1):347.
42. Shu S, Cui H, Liu Z, Zhang H, Yang Y, Chen X, et al. Suppression of RCAN1 alleviated lipid accumulation and mitochondrial fission in diabetic cardiomyopathy. Metab Clin Exp. 2024;158:155977.
43. Chang P, Zhang X, Zhang J, Wang J, Wang X, Li M, et al. BNP protects against diabetic cardiomyopathy by promoting Opa1-mediated mitochondrial fusion via activating the PKG-STAT3 pathway. Redox Biol. 2023;62:102702.
44. Montaigne D, Marechal X, Coisne A, Debry N, Modine T, Fayad G, et al. Myocardial contractile dysfunction is associated with impaired mitochondrial function and dynamics in type 2 diabetic but not in obese patients. Circulation. 2014;130(7):554–64.
45. Larsen TD, Sabey KH, Knutson AJ, Gandy TCT, Louwagie EJ, Lauterboeck L et al. Diabetic pregnancy and maternal high-fat diet impair mitochondrial dynamism in the developing fetal rat heart by sex-specific mechanisms. Int J Mol Sci. 2019;20(12).
46. Cong J, Goll DE, Peterson AM, Kapprell HP. The role of autolysis in activity of the Ca^{2+}-dependent proteinases (mu-calpain and m-calpain). J Biol Chem. 1989;264(17):10096–103.
47. Lin J, Wang F, Jiang G, Zhang T, Zhang J, He Q, et al. LXR activation ameliorates high glucose stress-induced aberrant mitochondrial dynamics via downregulation of Calpain1 expression in H9c2 cardiomyoblasts. Biochem Biophys Res Commun. 2022;614:145–52.
48. Shi H, Yu Y, Liu X, Yu Y, Li M, Wang Y, et al. Inhibition of calpain reduces cell apoptosis by suppressing mitochondrial fission in acute viral myocarditis. Cell Biol Toxicol. 2022;38(3):487–504.
49. Gao Q, Tian R, Han H, Slone J, Wang C, Ke X, et al. PINK1-mediated Drp1(S616) phosphorylation modulates synaptic development and plasticity via promoting mitochondrial fission. Signal Transduct Target Ther. 2022;7(1):103.
50. Huang J, Xie P, Dong Y, An W. Inhibition of Drp1 SUMOylation by ALR protects the liver from ischemia-reperfusion injury. Cell Death Differ. 2021;28(4):1174–92.
51. Liu A, Hatch AL, Higgs HN. Effects of phosphorylation on Drp1 activation by its receptors, actin, and cardiolipin. bioRxiv: the preprint server for biology. 2023.
52. Ye X, Ren H, Zhang M, Sun Z, Jiang AC, Xu G. ERK1/2 signaling pathway in the release of VEGF from Muller cells in diabetes. Investig Ophthalmol Vis Sci. 2012;53(7):3481–9.
53. Cai J, Wang J, Huang Y, Wu H, Xia T, Xiao J, et al. ERK/Drp1-dependent mitochondrial fission is involved in the MSC-induced drug resistance of T-cell acute lymphoblastic leukemia cells. Cell Death Dis. 2016;7(11):e2459.
54. Feng W, Wang J, Yan X, Zhang Q, Chai L, Wang Q, et al. ERK/Drp1-dependent mitochondrial fission contributes to HMGB1-induced autophagy in pulmonary arterial hypertension. Cell Prolif. 2021;54(6):e13048.

Publisher's note